DOI: 10.18721/JPM.13407

THE ABDOMINAL AORTA BIFURCATION WITH ILIAC ARTERIES: THE WALL ELASTICITY EFFECT ON THE FLOW STRUCTURE

A.A. Kotmakova[1], Ya.A. Gataulin[2], A.D. Yukhnev[2], D.K. Zaitsev[2]

[1] Scientific Research Institute for Optoelectronic Instrument Engineering, Sosnovy Bor, Leningrad region, Russian Federation;

[2] Peter the Great St. Petersburg Polytechnic University, St. Petersburg, Russian Federation

For the first time, a numerical study of the effect of vascular elasticity on blood flow has been carried out using a model of the abdominal aorta bifurcation with iliac arteries of the average statistical geometry. The greatest effect of elasticity was shown to be observed in the abdominal aorta before bifurcation, where there are large deformations of the vessel walls, changing the shape of the cross section from oval to circular. Taking into account the elasticity of the walls, the flow structure remained unchanged, but the maximum flow rate increased by 40 % in the abdominal aorta. In the abdominal-aortic bifurcation region the time-averaged wall shear stress decreased by 20%, and their oscillatory shear index increased by 60%.

Keywords: abdominal aorta's bifurcation, numerical simulation, wall elasticity, blood flow structure

Citation: Kotmakova A.A., Gataulin Ya.A., Yukhnev A.D., Zaitsev D.K., The abdominal aorta bifurcation with iliac arteries: the wall elasticity effect on the flow structure, St. Petersburg Polytechnical State University Journal. Physics and Mathematics. 13 (4) (2020) 68–76. DOI: 10.18721/JPM.13407

Introduction

Circulatory system diseases are one of the major causes of death worldwide. Numerical simulation of blood flow in 3D artery models provides new data on the flow structure, which helps predict the development of vascular diseases due to hemodynamic causes.

The abdominal aorta is an artery that supplies blood to the abdominal cavity and lower extremities. Currently, studies of flow in the abdominal aortic bifurcation are performed both experimentally [1–3] and by numerical simulation methods [4–9]. Some studies consider flows in the abdominal aortic bifurcation with subsequent bifurcations of iliac arteries [6, 8, 9].

Numerical simulation of blood flow in three different models of abdominal aortic bifurcation with iliac arteries was performed in [6]; the models were built based on anatomical data of magnetic resonance angiography. Blood flow velocities were obtained in [7] from magnetic resonance imaging data; shear stress distributions at rest were analyzed for all three models. The data on pressure and blood flow velocities using both rigid and deformable abdominal aortic wall models were given in [8].

Notably, numerical studies of blood flow in the abdominal aorta are performed mainly for models with rigid walls [10, 11]. The rigid wall approximation is largely used because of the complexity of solving the computational problem of the relationship between blood flow and vessel deformation. Such an approximation is justified by the fact that wall deformations do not significantly change the velocity field under normal conditions. It is used for arteries with small wall pulsations, but it may not be acceptable for arteries with large deformations (e.g., the thoracic or abdominal aorta). Clinical studies [12, 13] obtained the displacements of the abdominal aortic wall reaching 4–10%.

Analysis of the literature showed that most computational studies with 3D models of the abdominal aorta with iliac arteries use patient-specific models [8, 9], constructed based on clinical data. An abdominal aortic bifurcation model was used in [9], providing the flow pattern and the field of averaged shear stresses. However, the authors did not study the dependence of flow characteristics on wall elasticity.

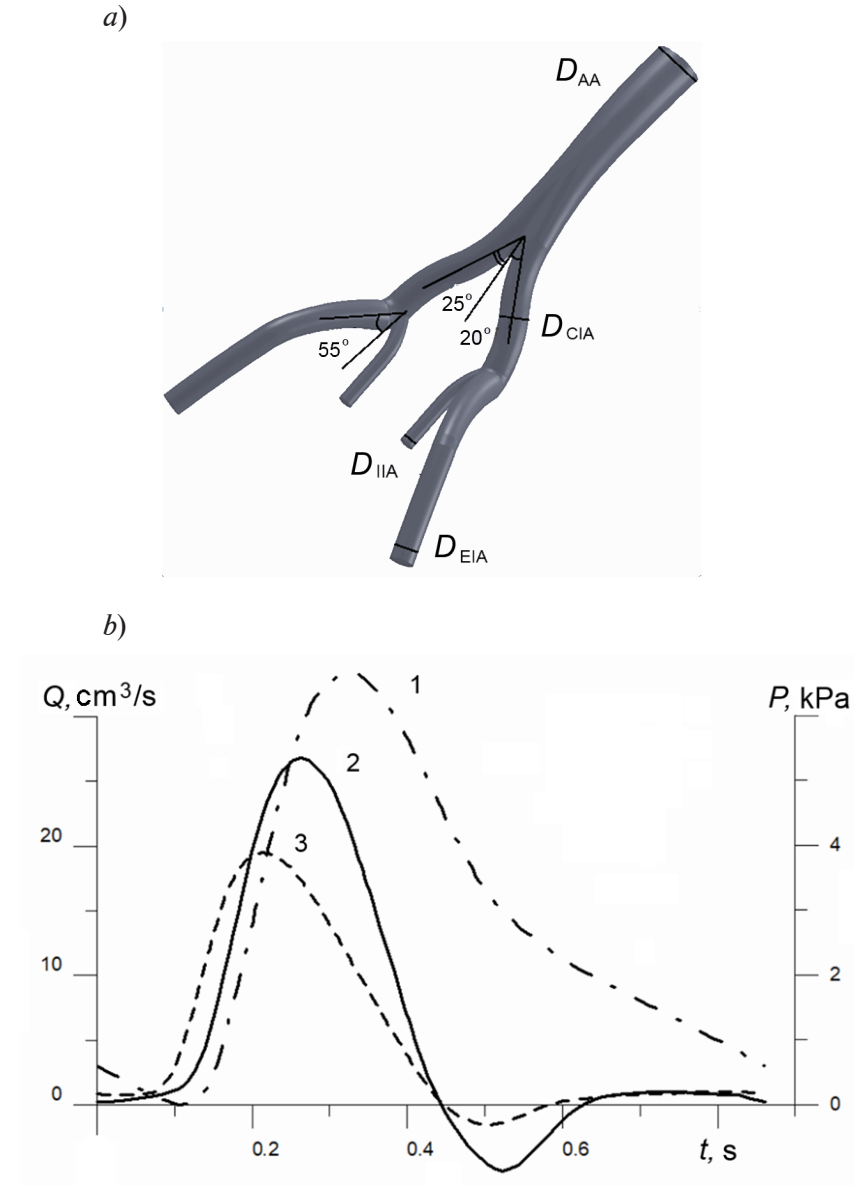

Fig. 1. Three-dimensional model of vessel bifurcation [14] (*a*) and graphical representation of boundary conditions for the mechanical (*1*) and hydrodynamic (*2*, *3*) problems posed (*b*).
The dynamics of the pulsatile component of pressure P on the inner wall of the abdominal aorta (AA) (*1*) and flow rates Q at the outlet of the external (EIA) (*2*) and internal (IIA) (*3*) iliac arteries; D_{CIA} is the diameter of the common iliac artery

Table

Geometric characteristics of the abdominal aortic bifurcation model

Bifurcation segment	Inlet diameter D_{in}, mm	Outlet diameter D_{out}, mm	Vessel length L, mm
Abdominal aorta (AA)	18.0	15.5	85
Left and right iliac arteries:			
common (CIAs)	10.8	10.8	46
external (EIAs)	10.8	9.0	62
internal (IIAs)	5.5	5.5	38

Parametric flow computations in models of blood vessels of average geometry help answer the question whether the wall deformation should be taken into account in patient-specific models or the changes in the flow structure during wall deformation are insignificant and can be neglected without significant loss of accuracy.

This work investigates the influence of wall elasticity on the structure of flow in a model of abdominal aortic bifurcation with iliac arteries of average statistical three-dimensional geometry. We analyzed the influence of the above elasticity on the structure of cross flow as well as on the shear stress magnitude and oscillatory shear index.

Geometric model of abdominal aortic bifurcation

In the present study, we used the model of abdominal aortic bifurcation with iliac arteries (Fig. 1,*a*) from [14], where its construction is described in detail based on averaged clinical data. The model includes the abdominal aorta, right and left common iliac arteries, right and left internal and external iliac arteries.

The geometric characteristics of the model are shown in Table. The deviation from the outlet axis of the abdominal aorta is 25° and 20° for the left and right iliac arteries, respectively. The angle between the internal iliac artery and the plane of the external iliac arteries is 55°.

Mathematical model

The simulation of fluid and wall motion was performed using the Fluid-Structure Interaction (FSI) technology, implemented as a one-way FSI data transfer. The flow in the abdominal aortic bifurcation with the iliac arteries was simulated by solving unsteady 3D Navier-Stokes equations for an incompressible viscous fluid on a deformable mesh. The computations were performed in the ANSYS CFX program with second-order spatial and temporal accuracy. The equation of motion for the solid wall was solved in the ANSYS Transient Structural program based on the finite element method. Data transfer between solvers was performed in the ANSYS System Coupling module, which transfers data on pressure and motion between ANSYS CFX and ANSYS Transient Structural. A mechanical problem is solved at each time step, with the overpressure P, which is the difference between the instantaneous pressure and the minimum (diastolic) pressure, applied to the inner wall (Fig. 1,*b*). Next, wall displacement are automatically transferred to the hydrodynamic problem, where fluid flow in the deformed model is computed, and then the next time step is processed.

The boundary conditions were obtained by averaging clinical data recorded in fifteen patients using magnetic resonance imaging [15–20]. A constant pressure level is set at the inlet to the abdominal aorta, and four pulsatile flow rates, the same for the left and right branches, are set at the outlet (see Fig. 1,*b*). The pulsation period is 0.86 s, which corresponds to a normal resting heart rate (70 bpm). The fluid is considered to be incompressible Newtonian, with the properties similar to those of human blood: density of 1000 kg/m^3, dynamic viscosity of 0.004 Pa·s.

The Reynolds number Re at the inlet to the abdominal aorta is equal to 1600 at the moment of maximum flow, the Womersley number Wo is equal to 24.3. These numbers are expressed as

$$\mathrm{Re} = \frac{Ud}{\nu}, \mathrm{Wo} = d\sqrt{\frac{2\pi}{\nu T}},$$

where U, m/c, is fluid velocity; d, m, is the aortic diameter; ν, m^2/s, is the kinematic viscosity of blood; T, s, is the pulsation period.

Mechanical characteristics of the abdominal aorta

The displacements of the cylindrical tube wall were computed using an isotropic elastic wall model. The wall thickness was taken to be 1 mm [21], its density 1000 kg/m^3, Poisson's ratio $\mu = 0.4$ [22]. It was assumed that the walls at the inlet and outlet were rigidly fixed.

The reference value of Young's modulus of the wall was taken as $E = 1$ MPa, it was chosen so that the wall deformation in the middle of abdominal aorta at maximum applied pressure P (see Fig. 1, *b*) was about 5%, which corresponds to physiological level of wall pulsation [20]. To estimate the value of Young's modulus, we used the following analytical formula [20]:

$$E = P\frac{R_0}{h_0}\left(1-\frac{\mu}{2}\right)\left(\frac{R_0}{R}-\frac{R_0^2}{R^2}\right)^{-1}, \qquad (1)$$

where R, R_0 are radii of the tube's medial surface at maximum (systolic) and minimum (diastolic) pressure, respectively; h_0 is the thickness of the tube wall.

In addition to the basic value of Young's modulus $E = 1$ MPa, computations were carried out for values $E = 2$, 4, 8 MPa and the problem with a rigid wall ($E \to \infty$).

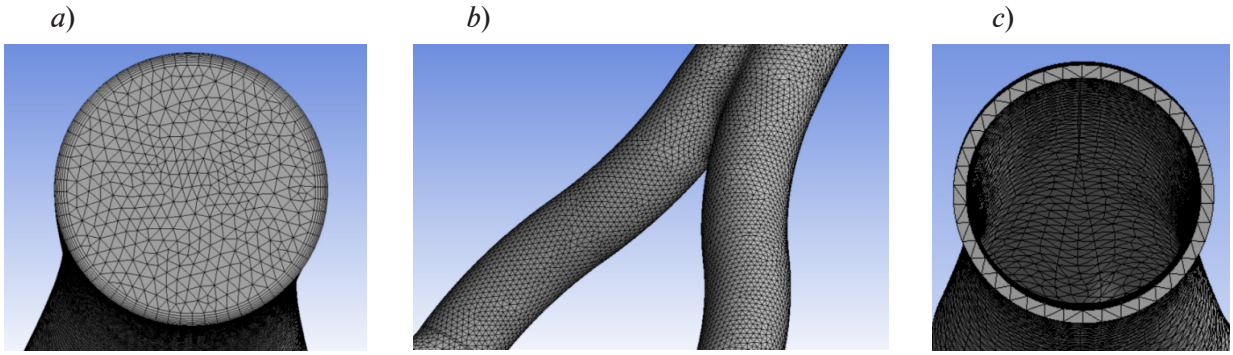

Fig. 2. Computational meshes used for the fluid (*a*) and for the wall (*b*, *c*)

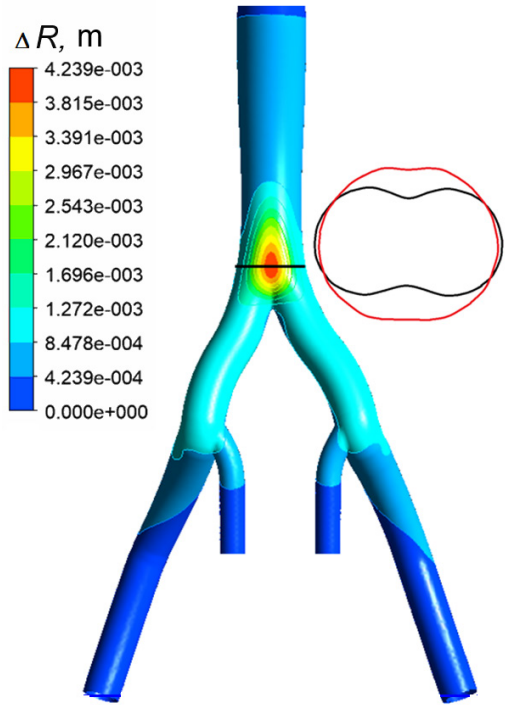

Fig. 3. Field of computed displacements of the elastic model wall at the moment of maximum pressure (rear wall view); boundaries of the vessel cross section at the moments of maximum (red line) and minimum (black line) pressure. Reference value of Young's modulus $E = 1$ MPa

Computational aspects

The CFD mesh (Fig. 2) consists of tetrahedra and has a layer of prismatic cells clustered to the wall. The computational mesh for the vessel wall also consists of tetrahedra. A study of mesh and time convergence was carried out for both meshes; as a result, a mesh of 0.8 million elements was used for CFD computations, and a mesh of 50,000 elements for the vessel wall. The time step was 0.01 s. Three periods were computed for all variants in order to exclude the influence of initial conditions.

Computational results and discussion

Wall displacements. Fig. 3 shows computed wall displacements at $E = 1$ MPa at the moment of maximum pressure P (see Fig. 1,*b*). Evidently, the maximum displacements are observed just before the abdominal aortic bifurcation, where the initial oval cross section of the vessel tends to take a circular shape.

The maximum displacements in the middle of the abdominal aorta are 5%, which corresponds to the preliminary estimate by Eq. (1) and justifies the choice of the basic value of Young's modulus ($E = 1$ MPa).

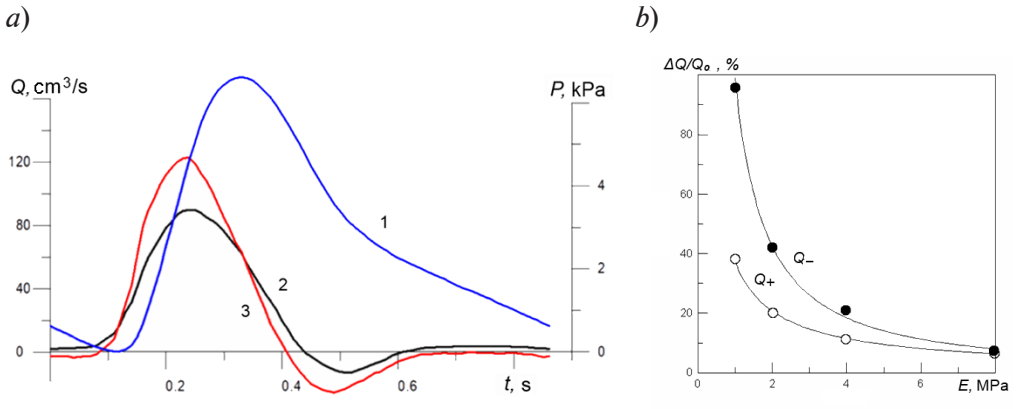

Fig. 4. Evolution of pulsatile component of pressure (*1*) on the inner wall of the vessel model (mechanical problem) and flow at the inlet to the abdominal aorta computed for rigid (*2*) and elastic (*3*) walls at $E \to \infty$ and 1 MPa, respectively (CFD problem) *(a)*; dependences of relative increase in amplitudes of positive (Q_+) and negative (Q_-) flow waves on Young's modulus (*b*)

Flow rate. Fig. 4,*a* shows the time evolution of the computed flow rate at the inlet to the abdominal aorta for the model with rigid ($E \to \infty$) and elastic (E = 1 MPa) walls. The elasticity of the walls increases the amplitude of both positive and negative flow waves. As the pressure increases, the walls of the vessel stretch, the cross-sectional area increases, and therefore the flow rate in the elastic model exceeds that of the rigid-wall model. As the pressure decreases, the walls contract, the cross-sectional area decreases, and the fluid is pushed out of the vessel: the negative flow rate increases, compared to the flow rate for the vessel with rigid walls. In addition, the duration of the positive flow phase decreased by 0.1 s for the deformed vessel (respectively, the duration of the negative flow phase increased by 0.1 s). The effect of Young's modulus on the change in the amplitude of positive (Q_+) and negative (Q_-) flow waves, compared with the results of the model with rigid walls, is shown in Fig. 4,*b*. The increase in amplitudes for the elastic model with E = 1 MPa was 40 and 95%, respectively.

Longitudinal velocity. Fig. 5 shows the fields of longitudinal velocity V_n (in the projection on the direction of the main flow) in three sections for the phases of increasing, maximum and decreasing pressure for models with rigid and elastic (E = 1 MPa) walls. It can be seen that the longitudinal velocity profile has an irregular shape in all cases. The velocity in the abdominal aorta (yellow section) is higher on the anterior wall, since this wall is external to the curved abdominal aorta. In the second part of the decreasing pressure phase, backflow is observed. The pattern of the longitudinal velocity field in the section before the bifurcation is similar to that in the middle of the abdominal aorta, but the velocities are increased. Maximum for the longitudinal velocity in the common iliac artery is shifted toward the inner wall of the artery in the positive flow phase, while in the negative phase, on the contrary, it is shifted toward the outer wall. There is flow separation at the external wall of the common iliac artery at the moment of maximum pressure.

During the phase of increasing pressure (at the moment of maximum flow), the maximum cross-sectional longitudinal velocity *Vn* in the elastic-wall model is higher than in the rigid-wall model by about 15% in the abdominal aorta, and by 2% in the common iliac artery. During the phase of decreasing pressure, the longitudinal backflow velocity in the elastic-wall model is higher for the elastic model: by 25% in the abdominal aorta and by 15% in the common iliac artery.

Transverse velocity. Fig. 6 shows the streamlines in three cross sections for models with rigid ($E \to \infty$) and elastic (E = 1 MPa) walls. Dean's vortices appear in the given sections of bifurcations of the abdominal aorta and iliac arteries due to the curvature of the vessels. In this case, the same vortex structure of the flow is observed in both rigid and elastic models, differing only by the values of the transverse flow velocity due to stretching of the vessel walls. The maximum values of transverse velocity for the elastic model exceed those for the rigid model by about 10%.

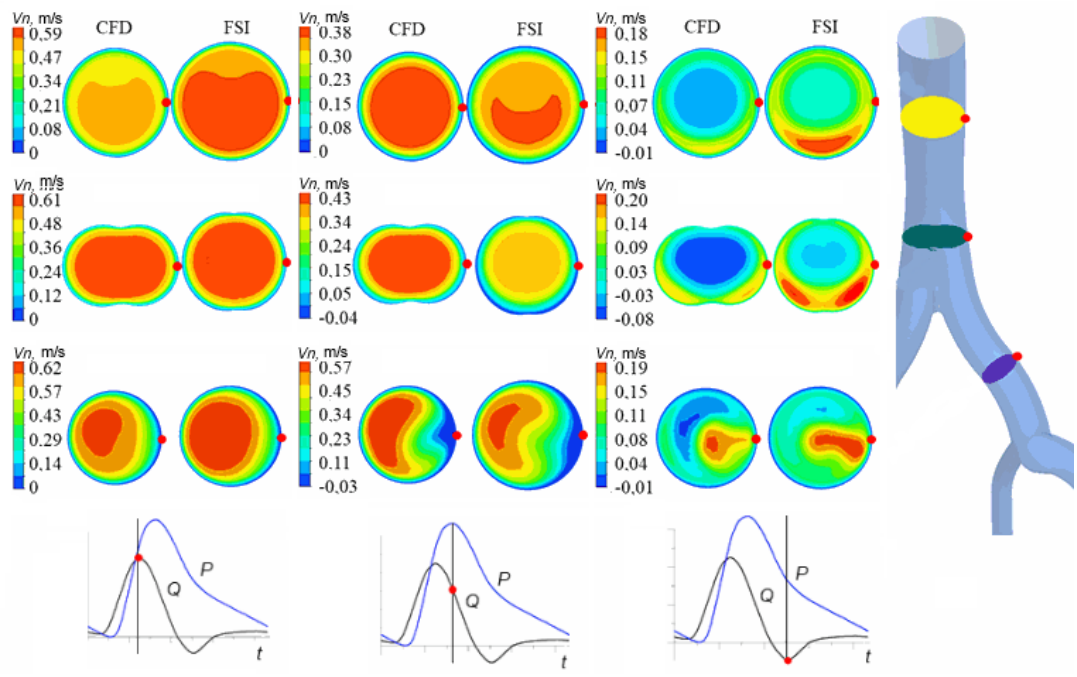

Fig. 5. Patterns of longitudinal velocity fields in three cross sections in different phases of the cycle, computed for rigid (CFD, $E \to \infty$) and elastic (FSI, $E = 1$ MPa) models of the abdominal aorta; the dimensions of the cross sections are conventionally shown as equal, the pressures and flow rates for the three phases of the cycle are marked at the bottom of the figure

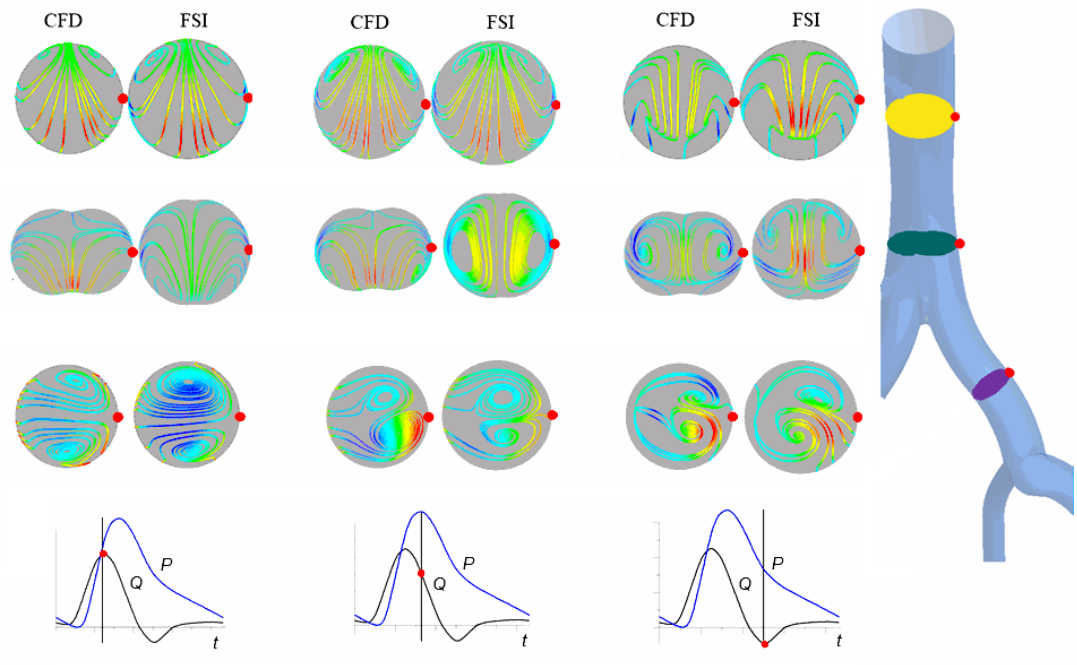

Fig. 6. Streamlines in three cross sections in different phases of the cycle, computed for rigid (CFD, $E \to \infty$) and elastic (FSI, $E=1$ MPa) models of abdominal aortic bifurcation; the dimensions of arterial cross-sections are conventionally shown as equal, the pressures and flow rates for the three phases of the cycle are marked at the bottom of the figure

Wall shear stress. It is known that regions with low shear stresses and high oscillatory shear index on the vessel wall are associated with formation and development of atherosclerosis. Lower (dangerous from the standpoint of atherosclerosis development) shear stresses on the wall are observed in the regions where flow separation occurs. High values of oscillatory shear index are also observed there. To assess the influence of wall elasticity on shear stresses, TAWSS (Time-Averaged Wall Shear Stress) and OSI (Oscillatory Shear Index) values were calculated for rigid and elastic models:

$$\mathrm{OSI} = \frac{1}{2}\left(1 - \frac{\left|\int_0^T \boldsymbol{\tau}_w dt\right|}{\int_0^T |\boldsymbol{\tau}_w| dt}\right),$$

$$\mathrm{TAWSS} = \frac{1}{T}\int_0^T |\boldsymbol{\tau}_w| dt,$$

where $\boldsymbol{\tau}_w$ is the vector of wall shear stress; t, s, is the time; T, s, is the pulsation period.

Fig. 7,*a* shows the distributions of time-averaged wall shear stress and the oscillatory shear index on the abdominal aortic bifurcation wall in the rigid ($E \to \infty$) and elastic (E = 1MPa) models. The effect of Young's modulus on these characteristics is shown in Fig. 7,*b*. The greatest difference in shear stresses (20% less in the elastic model, compared to the rigid model) is observed in the abdominal aorta, in the location of the greatest wall deformation. A minor difference (the difference does not exceed 10% in the elastic model relative to the rigid model) is observed in the external iliac arteries; in the remaining parts of the abdominal aorta, the influence of its wall elasticity on the averaged shear stresses does not exceed 2%.

The greatest difference between the values of the oscillatory shear index (OSI) is observed before the abdominal aortic bifurcation: the OSI value for the elastic model (on average over the circumference) is higher than the data for the rigid model by approximately 60%. Smaller differences from the rigid model are observed in the iliac arteries: OSI values for the elastic model are 10% higher.

Conclusion

The influence of wall elasticity on blood flow in the bifurcation of the abdominal aorta with iliac arteries of the average statistical geometry was investigated using numerical simulation. The maximum wall deformation in the middle of the abdominal aorta was 5%, which corresponds to the physiological level of wall pulsation. The greatest influence of elasticity is observed in the region immediately before the bifurcation,

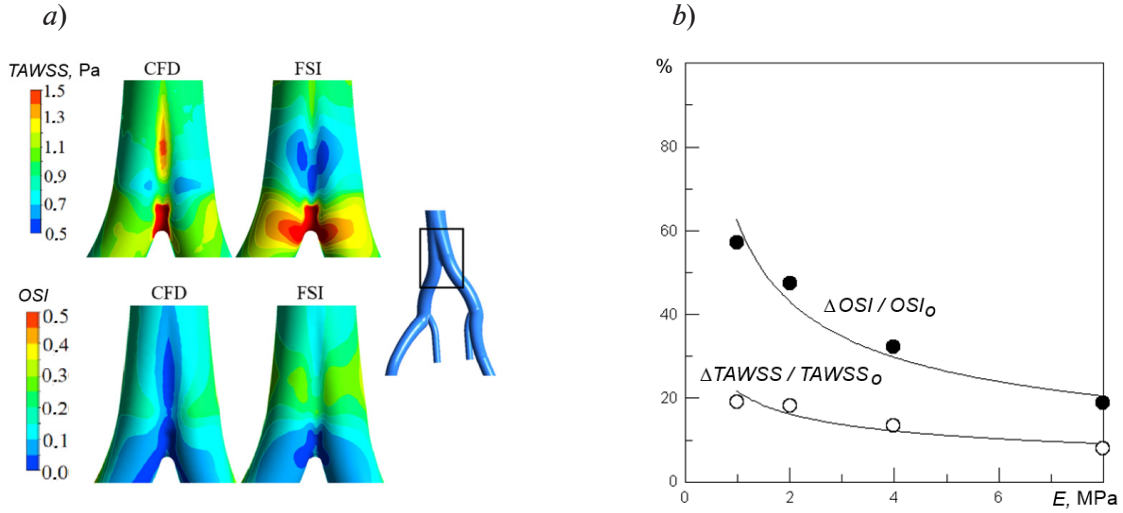

Fig. 7. Computations for two models (CFD and FSI) for the time-averaged wall shear stress (TAWSS (I)) and oscillatory shear index (OSI (II)) in the abdominal aortic bifurcation (*a*); dependences of relative differences of the above characteristics, I and II, on Young's modulus values (*b*)

Rigid (CFD, $E \to \infty$) and elastic (FSI, E = 1 MPa) models were used, the index "o" marks the characteristics of the rigid model

where there are large deformations of the vessel walls, changing the shape of the cross section from oval to circular.

According to the results obtained, the structure of transverse flow along the vessel has no qualitative differences for elastic and rigid bifurcation models. We have found that the maximum values of transverse velocity for the elastic model are about 10% higher than for the rigid model.

Due to the change in the cross-sectional area of the vessel resulting from the deformation of the walls, the flow rate increases at the phase of increasing pressure and decreases with decreasing pressure. Comparative analysis of the obtained results showed that the amplitude of the forward flow rate increased by 40% for the elastic model, while that of the backflow rate almost doubled.

The time-averaged wall shear stress (TAWSS) decreased by 20% in the bifurcation region for the model with elastic walls, and oscillatory shear index (OSI) increased by 60%.

This work was supported financially by the Russian Foundation for Basic Research (grant no. 18-01-00629).

REFERENCES

1. **Chong C.K., How T.V.,** Flow patterns in an endovascular stent-graft for abdominal aortic aneurysm repair, Journal of Biomechanics. 37(1) (2004) 89–97.

2. **Ku D.N., Glagov S., Moore Jr. J.E., Zarins C.K.,** Flow patterns in the abdominal aorta simulated postprandial and exercise conditions: an experimental study, Journal of Vascular Surgery. 9 (2) (1989) 309–316.

3. **Gataulin Ya.A., Zaitsev D.K., Smirnov E.M., Fedorova E.A., Yukhnev A.D.,** Weakly swirling flow in a model of blood vessel with stenosis: Numerical and experimental study, St. Petersburg State Polytechnical University Journal. Physics and Mathematics. (4(230)) (2015) 36–47.

4. **Gataulin Ya.A., Zaitsev D.K., Smirnov E.M., Yukhnev A.D.** Numerical study of spatial-temporal evolution of the secondary flow in the models of a common carotid artery, St. Petersburg State Polytechnical University Journal. Physics and Mathematics. (4 (253)) (2016) 48–55.

5. **Gataulin Y.A., Yukhnev A.D., Zaitsev D.K., et al.,** Structure of the secondary flow in the bifurcation of a blood vessel: patient specific modeling and clinical Doppler measurements, Journal of Physics: Conference Series. 1135 (2018) 012089.

6. **Dalman R.L., Tedesco M.M., Myers J.,** AAA disease: mechanism, stratification, and treatment, Annals of the New York Academy of Sciences. 1085(1) (2006) 92–109.

7. **Tang B.T., Cheng C.P., Tsao P.S., Taylor C.A.,** Subject-specific finite element modeling of three-dimensional pulsatile flow in the human abdominal aorta: comparison of resting and exercise conditions, Proceedings of the 2003 Summer Bioengineering Conference, June 25 – 29, 2003, Sonesta Beach Resort, Key Biscayne, **Florida**, USA (2003) 2.

8. **Figueroa C.A., Vignon-Clementel I.E., Jansen K.E., et al.,** A coupled momentum method for modeling blood flow in three-dimensional deformable arteries, Computer Methods in Applied Mechanics and Engineering. 195(41) (2006) 5685–5706.

9. **Ke L., Wentao J., Yu** C., **et al.,** Fluid-solid interaction analysis on iliac bifurcation artery: a numerical study, International Journal of Computational Methods. Chengdu, China.17. 16 (7) (2019) 1850112.

10. **Javadzadegan A., Simmons A., Barber T.,** Spiral blood flow in aorta-renal bifurcation models, Computer Methods in Biomechanics and Biomedical Engineering. 19(9) (2015) 964–976.

11. **Mesri Y., Niazmand H., Deyranlou A.,** Numerical study on fluid-structure interaction in a patient-specific abdominal aortic aneurysm for evaluating wall heterogeneity and material model effects on its rupture, Journal of Applied Fluid Mechanics. 10(6) (2017) 1699–1709.

12. **Ahlgren A.R., Hansen F., Sonesson B., Lanne T.,** Stiffness and diameter of the common carotid artery and abdominal aorta in wmen, Ultrasound in Medicine and Biology. 23 (7) (1997) 983–988.

13. **Koullias G., Modak R., Tranquilli M., et al.,** Mechanical deterioration underlies malignant behavior of aneurysmal human ascending aorta, The Journal of Thoracic and Cardiovascular Surgery. 130 (3) (2005) 677–683.

14. **Sinitsyna D.E., Yukhnev A.D., Zaitsev D.K., Turkina M.V.,** The flow structure in a three-dimensional model of abdominal aortic bifurcation: ultrasonic and numerical study, St. Petersburg State Polytechnical University Journal. Physics and Mathematics. 12 (4) (2019) 50–60.

15. **Yeung J.J., Kim H.J., Abbruzzese T.A., et al.,** Aortoiliac hemodynamic and morphologic adaptation to chronic spinal cord injury, Journal of Vascular Surgery. 44 (6) (2006) 1254–1265.

16. **Malossi A.C.I., Bonnemain J.,** Numerical comparison and calibration of geometrical multiscale models for the simulation of arterial flows, Cardiovascular Engineering and Technology. 4 (4) (2013) 440 –463.

17. **Alimohammadi M., Pichardo-Almarza C., Tomaso G., et al.,** Predicting atherosclerotic plaque location in an iliac bifurcation using a hybrid CFD/biomechanical approach, Lecture Notes in Computer Science: Bioinformatics and Biomedical Engineering, Part II, Eds. Ortuco F., Rojas I. 9044 (2015) 594–606.

18. **Xiao N.,** Simulation of 3-D blood flow in the full systemic arterial tree and computational frameworks for efficient parameter estimation, A dissertation submitted to Stanford University for the degree of PhD, Stanford, 2014. www.isd.ksl.ac.uk/FigueroaLabFiles/papers/NX-thesis.

19. **Long Q., Xu X.Y., Bourne M., Griffith T.M.,** Numerical study of blood flow in an anatomically realistic aortic-iliac bifurcation generated from MRI data, Magnetic Resonance in Medicine. 43 (4) (2000) 565–576.

20. **Tang B.T., Cheng C.P., Draney M.T., et al.,** Abdominal aortic hemodynamics in young healthy adults at rest and during lower limb exercise: quantification using image-based computer modeling, American Journal of Physiology Heart and Circulatory Physiology. 291(2) (2006)668–676.

21. **Schriefl A.J., Zeindlinger G., Pierce D.M., et al.,** Determination of the layer-specific distributed collagen fibre orientations in human thoracic and abdominal aortas and common iliac arteries, Journal of the Royal Society Interface. 9 (71) (2012) 1275–1286.

22. **Mbodj C., Altnji H.E., Bou-Said B., Walter-Le Berre H.,** Analysis of the phenomenon of endoleak of type I A. Influence of the mechanical characterization of the aorta, Journal of Hypertension and Management. 2 (1) (2016) 1510014.

23. **Begun P.I., Afonin P.N.,** Modelirovaniye v biomekhanike [Modeling in biomechanics], Vysshaya shkola, Moscow, 2004 (in Russian).

Received 01.10.2020, accepted 30.10.2020.

THE AUTHORS

KOTMAKOVA Anna A.
Scientific Research Institute for Optoelectronic Instrument Engineering
29 Leningradskaya St., Sosnovy Bor, Leningrad region,188540, Russian Federation
www.anechka_kotmakova@mail.ru

GATAULIN Yakov A.
Peter the Great St. Petersburg Polytechnic University
29 Politechnicheskaya St., St. Petersburg, 195251, Russian Federation
yakov_gataulin@mail.ru

YUKHNEV Andrey D.
Peter the Great St. Petersburg Polytechnic University
29 Politechnicheskaya St., St. Petersburg, 195251, Russian Federation
a.yukhnev@mail.ru

ZAITSEV Dmitri K.
Peter the Great St. Petersburg Polytechnic University
29 Politechnicheskaya St., St. Petersburg, 195251, Russian Federation
zaitsev-aero@yandex.ru